The Mechanism of Lamellar-to-Inverted Hexagonal Phase Transitions: A Study using Temperature-Jump Cryo-Electron Microscopy

D. P. Siegel,* W. J. Green,* and Y. Talmon‡

*Procter & Gamble Co., Miami Valley Laboratories, Cincinnati, Ohio 45239–8707 USA; ‡Department of Chemical Engineering, Technion–Israel Institute of Technology, Haifa 32000, Israel

ABSTRACT The lamellar/inverted hexagonal (L_α/H_{II}) phase transition can be very fast, despite the drastic change in the topology of the lipid/water interfaces. The first structures to form in this transition may be similar to those that mediate membrane fusion in many lipid systems. To study the transition mechanism and other dynamic phenomena in membrane dispersions, we constructed an apparatus to rapidly trigger the transition and then vitrify the specimens to preserve the structure of transient intermediates. The apparatus applies millisecond-long temperature jumps of variable size to aqueous dispersions of lipids on electron microscope grids at times 9–16 ms before specimen vitrification. The vitrified specimens are then examined by cryo-transmission electron microscopy. Dispersions of egg phosphatidylethanolamine completed the transition within 9 ms when superheated by 20 K. Similar transition times have been observed in dioleoylphosphatidylethanolamine via time-resolved x-ray diffraction. N-monomethylated dioleoylphosphatidylethanolamine dispersions superheated to lesser extent exhibited slower transitions and more complex morphology. The structure of the first intermediates to form in the transition process could not be determined, probably because the intermediates are labile on the time scale of sample cooling and vitrification (<1 ms) and because of the poor contrast developed by some of these small structures. However, the results are more compatible with a transition mechanism based on "stalk" intermediates than a mechanism involving inverted micellar intermediates. Temperature-jump cryo-transmission electron microscopy should be useful in studying dynamic phenomena in biomembranes, large protein complexes, and other colloidal dispersions. It should be especially helpful in studying the mechanism of protein-induced membrane fusion.

INTRODUCTION

The mechanisms of lamellar/inverted hexagonal (L_α/H_{II}) and lamellar/inverted cubic (L_α/Q_{II}) transitions are of interest for two reasons. First, drastic rearrangements in the topology of the lipid/water interfaces must occur in these transitions. These rearrangements probably require energy-intensive processes, which would result in slow overall rates. Yet some of these transitions can be quite rapid. Second, many authors have suggested that the first structures to form during these transitions are related to the structures that mediate membrane fusion in liposomal systems (for reviews and specific mechanisms, see Verkleij, 1984; Siegel, 1986a; Siegel, 1993).

To determine the mechanism of the phase transition, one must determine the structure of the intermediates that form during the process. Many authors have imaged structures associated with L_α/H_{II} and L_α/Q_{II} phase transitions, using freeze-fracture electron microscopy (FFEM; e.g., Verkleij et al., 1980; Van Venetië and Verkleij, 1981; Hui et al., 1983; reviewed in Verkleij, 1984) or cryo-electron microscopy (Frederik et al., 1989, 1991; Siegel et al., 1989). However, it has not been possible to unambiguously determine the transition mechanism on the basis of those results.

Two L_α/H_{II} phase transition mechanisms have been proposed, requiring intermediate structures of different geometries. These two mechanisms should be distinguishable on the basis of time-resolved transmission electron microscopy (TRC-TEM) data (intermediate morphology and intermediate formation time scales). The first mechanism is based on formation of inverted micellar structures (IMIs) (Verkleij et al., 1980). These structures (Siegel, 1984; 1986a) form between two apposed lipid bilayers. IMIs consist of a spherical inverted micelle contained within a semitoroidal outer monolayer connecting the interfaces of the two original bilayers. IMIs are 10–12 nm in diameter at the narrowest point. On the basis of FFEM data, IMIs were postulated to form H_{II} tubes by aggregation in strings between apposed bilayers (Verkleij et al., 1980). Siegel (1986a) proposed that pairs of IMIs could also form structures known as line defects (LDs) that rapidly elongate and align into H_{II} tube arrays. The ends of these line defects would resemble IMIs.

Received for publication 30 August 1993 and in final form 15 November 1993.

Address reprint requests to Dr. David Siegel, Procter & Gamble Co., Miami Valley Laboratories, P. O. Box 398707, Cincinnati, OH 45239–8707.

Abbreviations used: CEVS, controlled environment vitrification system; cryo-TEM, cryo-transmission electron microscopy; d_{11} and d_{20}, spacing of the 11 and 20 lattice planes in the H_{II} phase; DOPC, dioleoylphosphatidylcholine; DOPE, dioleoylphosphatidylethanolamine; DOPE-Me, N-monomethylated dioleoylphosphatidylethanolamine; DSC, differential scanning calorimetry; EDTA, ethylenediamine tetraacetic acid; EM, electron microscopy; FFEM, freeze-fracture electron microscopy; H_{II}, inverted hexagonal phase; ILA, interlamellar attachment; IMI, inverted micellar intermediate; L_α, lamellar liquid crystalline phase; LD, line defect; LUV, large unilamellar vesicle; PFN, pulse-forming network; Q_{II}, inverted cubic phase; son-LUV, sonicated LUV; TPE, phosphatidylethanolamine obtained by transphosphatidylation of egg phosphatidylcholine; TRC-TEM, time-resolved cryo-TEM.

0006-3495/94/02/402/13 $2.00

In the second type of proposed transition mechanism, the first structures to form are so-called stalks, which are catenoidal connections between the interfaces of apposed bilayers (Markin et al., 1984; Siegel, 1993), and should have a diameter of only ~4 nm at their narrowest point. Hui et al. (1983) proposed that structures equivalent to stalks (conical lipidic particles in their terminology) could elongate directly into LDs, a process explored in more detail by Siegel (manuscript in preparation). Caffrey (1985) also proposed a mechanism that requires LD-like intermediates. The LDs in such a mechanism would have ends resembling halves of stalks, much smaller than the IMI ends expected in an IMI-mediated transition. Stalk-mediated transitions should be inherently faster than IMI-mediated transitions. Theoretical work (Siegel, 1986a) indicates that in the IMI-mediated mechanism LD growth is by far the fastest means of H_{II} phase production. However, LDs are produced by aggregation and fusion of IMIs, whereas in the stalk-mediated transition the first structures to form are immediately capable of elongating into LDs.

Many lipid systems form isotropic or inverted cubic phases near the L_α/H_{II} phase boundary (Lindblom and Rilfors, 1989). Electron micrographic data (Siegel et al., 1989) indicate that these phases arise from structures known as interlamellar attachments (ILAs; Siegel, 1986a,b), which are catenoidal bilayer connections between apposed L_α phase lamellae. A candidate L_α/H_{II} transition mechanism should be able to generate this entire manifold of recorded structures on observed transition time scales. Both IMIs (Siegel, 1984, 1986a,b) and stalks (Markin et al., 1984; Siegel, 1993) are capable of forming ILAs. However, theoretical calculations (Siegel, 1986b,c) suggest that the IMI-mediated transition mechanism would generate ILAs comparatively slowly (on the order of 1 s), whereas stalks should be able to form ILAs on much faster time scales (Siegel, 1993). A previous study (Siegel et al., 1989) demonstrated only that ILAs formed within ~1 s or less.

Therefore, TRC-TEM could distinguish between the two proposed transition mechanisms in three ways. First, IMIs and stalks have very different structures. If unambiguous evidence for either structure is obtained, this alone would determine which mechanism is the better candidate. Second, actively elongating LDs should have ends that resemble the structures that formed them (IMIs or stalks). Inconclusive evidence for LD structure exists (Van Venetië and Verkleij, 1981; Hui et al., 1983), and the structure of the ends of the LDs has not been established. Last, TRC-TEM should indicate how rapidly ILAs form. As discussed above, a stalk-mediated transition would be expected to generate such structures on millisecond or sub-millisecond time scales, compared with ~1 s for an IMI-mediated mechanism (Siegel, 1986a,b).

Cryo-transmission electron microscopy (cryo-TEM; Dubochet et al., 1988) is particularly appropriate for studying lipid phase transitions. The specimens are ~0.1-μm-thick films of aqueous dispersions, so vitrification is particularly fast and efficient, and it is more likely that highly transient structures will be fixed in more specimens with this technique than with FFEM. Cryo-TEM images are two-dimensional projections of all the membranes in a dispersion, whereas FFEM images only a single fracture surface. It is therefore easier to image rare, short-lived intermediate structures with cryo-TEM. The disadvantage of cryo-TEM is that images of lipidic structures in water are often formed with comparatively poor contrast. Therefore, cryo-TEM is an excellent complementary technique to FFEM. To image early intermediates in dynamic phenomena, TRC-TEM was developed. In this technique, the dynamic phenomenon of interest is triggered on the electron microscope grid just before vitrification, either by mixing reactant solutions (Siegel et al., 1989; Talmon et al., 1990) or by a rapid increase in temperature (Chestnut et al., 1992). Previously, we used the on-the-grid mixing technique to study the mechanism of the L_α/Q_{II} phase transition and membrane fusion in systems near that phase boundary (Siegel et al., 1989). However, the specimen preparation apparatus in those studies could vitrify the specimens at times no shorter than ~1–3 s after triggering.

L_α/H_{II} phase transitions can occur in tens of milliseconds or less (Laggner et al., 1991; Tate et al., 1992). To maximize the probability of imaging transient intermediates in such rapid processes, one needs to trigger the process within milliseconds and vitrify the specimens milliseconds after that. In the present work, this was achieved by construction of an apparatus that induced variable sub-millisecond temperature jumps in cryo-TEM specimens 9–16 ms before vitrification. The peak sample temperature was chosen so that the specimens were at or above the L_α/H_{II} transition temperature, T_H, when they were plunged into the cryogen for vitrification. The temperature history of specimens processed in the apparatus was recorded using thermocouples fashioned from electron microscope grids (Clark et al., 1976).

MATERIALS AND METHODS

Temperature-jump apparatus

A diagram of the temperature-jump cryo-TEM specimen preparation system is presented in Fig. 1. The system makes use of many components of the CEVS (Controlled Environment Vitrification System) originally developed by Bellare et al. (1988). The CEVS chamber provides a temperature- and humidity-controlled enclosure in which the sample is prepared. A drop of the suspension is placed on the electron microscope grid and blotted to form a thin film, using filter paper wrapped around a flat metal wand applied to the grid from the rear for ~3 s. The grid is mounted in mini-serrefines (Fine Science Tools, Inc., Belmont, CA) attached to a spring-loaded plunger. An electromechanical shutter (Uniblitz model VSR25, A. W. Vincent Associates, Rochester, NY) is mounted on the bottom of the CEVS chamber. The plunger is triggered by a solenoid. The trigger assembly includes a safety interlock which prevents the plunger from moving unless the CEVS shutter is open. Mounted below the CEVS is a xenon flashtube (model L6119, ILC Technology, Sunnyvale, CA), which is depicted end-on in Fig. 1. The pulse-forming network (PFN; Fig. 1) is a tuned capacitive discharge circuit, including a custom high-current, high-voltage 600-μF capacitor (CSS type, High Energy Corp., Parkesburg, PA) triggered by a spark from a transformer circuit (model T105-B, ILC Technology). The molten ethane is maintained in a open vessel cooled with liquid nitrogen.

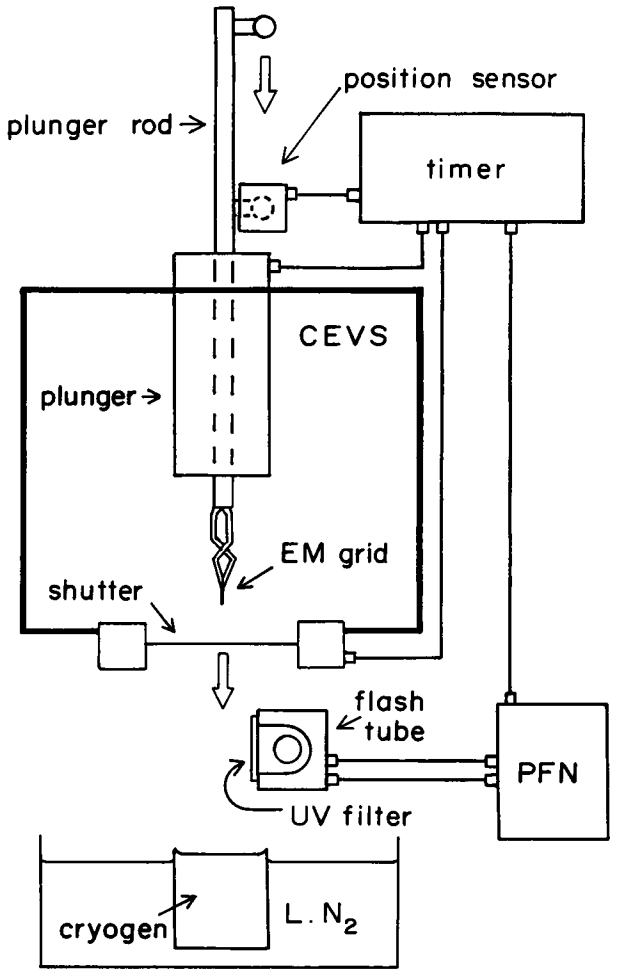

FIGURE 1 Diagram of the temperature-jump apparatus. CEVS denotes the temperature- and humidity-controlled chamber enclosing the electron microscope grid, which is mounted on a spring-loaded plunger. PFN indicates the capacitive discharge circuit that fires the flashtube.

When the timing circuitry is activated, the CEVS shutter opens and the plunger is triggered. The plunger rapidly accelerates to about 3.5 m/s, and the electron microscope grid moves toward the cryogen. When the grid is opposite the flash tube with the matte side of the grid in a face-on orientation (flashtube center-to-grid spacing of 2.0 cm), a position sensor on the plunger rod triggers the PFN, and the flashtube emits a brilliant 600-μs-long flash. This flash irradiates the electron microscope grid through a WG335 UV filter, which screens out wavelengths shorter than 335 nm that are potentially harmful to biological specimens.

A substantial fraction of the transmitted radiation is absorbed by the copper of the electron microscope grid, which heats rapidly. The water of the aqueous specimen absorbs almost no radiation in the visible band (Bayly et al., 1963) and absorbs very little infrared radiation. The flash tube in our apparatus emits only a few percent of its optical power in wavelengths longer than 1 μm (Technical Bulletin No. 3, ILC Technology). The wavelength range of maximum absorption by water is narrow and at substantially longer wavelengths (2.7–3.2 μm), and the ~0.2-μm-thick layer of water on the grid should absorb only about 10% of the power in that narrow band (using data from Bayly et al., 1963).

The aqueous film has a heat capacity that is only a few percent of the heat capacity of the metal grid. The combination of the relatively small heat capacity and optical clarity of the aqueous film means that the film has a very small effect on the flash-induced temperature jumps. This was demonstrated directly by thermocouple measurements (see below), in which grids with and without aqueous films heated to essentially the same temperatures. As a result, differences in the extent of blotting between different specimens should also have a negligible effect on the temperature jumps. Estimates using standard equations (Bird et al., 1960) indicate that the centers of aqueous films spanning the holes of 300-mesh electron microscope grids should reach 90% of the temperature jump applied to the metal within about 3 ms.

After illumination by the flash, the grid plunges into molten ethane. This "flash-to-splash" interval is determined by the size of the spring driving the plunger and is measured periodically with an oscilloscope and appropriate contact circuits. It was usually 9.2 ms in the present work. Under a blanket of cold nitrogen gas, the specimen is retrieved from the ethane and immediately immersed in liquid nitrogen. It is then transferred to an electron microscope and examined as described below.

Electron microscope grids

Three-hundred-mesh VECO copper electron microscope grids were obtained from E. F. Fullam, Inc. (Latham, NY) and were then modified by Dr. Ted Dunn of Ted Pella Inc. (Redding, CA) as follows. The matte sides of the grids were coated with a 0.2-μm-thick layer of platinum, and a lacy carbon substrate was then applied to the shiny sides. The platinum coating was applied to reduce the rate at which the grids tarnished during prolonged storage. Tarnishing changes the optical absorption coefficient of the metal, and thermocouple measurements (see below) indicate that this changes the peak temperature that grids reach after a flash of given intensity.

Calibration of the temperature jumps

Thermocouples were made from electron microscope grids (Clark et al., 1976). The grids were identical to the grids used for specimens, except that they lacked the lacy carbon substrate. (It was thought that the carbon substrate would interfere with the formation of good thermocouple junctions between the grids and the lead wires.) Copper and constantan wires of 0.001 inch in diameter (Omega Engineering, Stamford, CT) were woven three or four times through the mesh of the grids and pulled tight to give good electrical contacts and trimmed. The grids were then mounted in the apparatus and connected to thicker copper wires at points well away from the flashtube and cryogen. Sometimes the ends of the leads were micro-spot-welded to the grids to improve electrical contact. The output of the thermocouples was amplified through a DC amplifier (OmniAmp IIIA, Omega Engineering) operating at a cut-off frequency of 10 kHz and were recorded and analyzed using the EASYEST LX data analysis system (Keithley Instrument Co., Rochester, NY). The junctions were at room temperature, and the recorded EMF of the thermocouples at standard temperatures (ice water, boiling liquid nitrogen) agreed with values from calibration tables in the CRC Handbook of Chemistry and Physics (1991) to within less than ± 1°C, using measured room temperature as the junction temperature.

An example of the output is given in Fig. 2. The initial grid temperature was 21°C. The apparatus was triggered at $t = 0$. The transient at $t = 11$ ms is due to the plunger trigger solenoid firing. The flashtube fires at $t = 35$ ms (the radio frequency noise of the flashtube discharge induces a large transient), and the grid heats to 72°C in 1 ms. About 16 ms later, when the grid temperature has fallen to 62°C, the grid encounters the cryogen, which cools the grid at ~10^5 K/s. The time required to cool below the homogeneous nucleation temperature for ice (−40°C) is ~1 ms. This is the cooling time for the bulk of the metal grid; the aqueous films of the specimen come in direct contact with the molten ethane and may cool faster.

The magnitude of the initial temperature jump could be varied between at least 90 K and 20 K by adjusting the voltage on the capacitor in the PFN. The magnitude of the temperature jump was roughly proportional to the square of the capacitor voltage (or linearly proportional to the capacitor energy), as expected (data not shown). Oscilloscope measurements of flashtube light output (data not shown) showed that the pulse width did not change substantially across this voltage range. The reproducibility between flashes of the peak temperature for a given thermocouple is 1% or better. The reproducibility between different mountings of the same thermocouple or between different thermocouples, exposed to flashes of equivalent energy, are both approximately $\pm 15\%$. This variability is due to differences

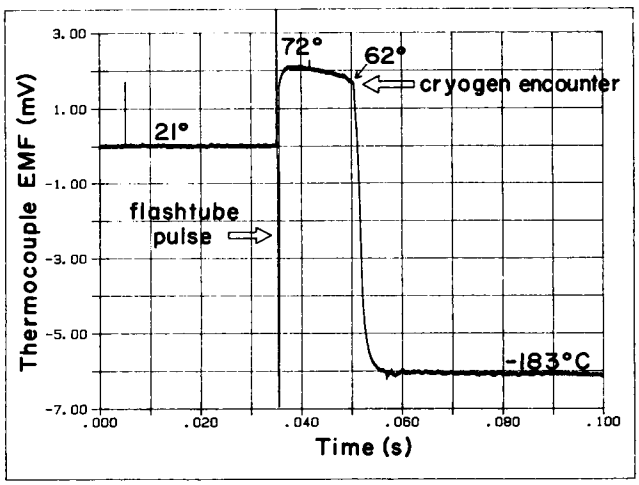

FIGURE 2 Electron microscope grid thermocouple voltage as a function of time during processing in the temperature-jump apparatus. The corresponding temperatures are marked at selected times.

in the extent of thermal contact with the forceps and (to a lesser extent) to grid-to-grid variations in weight and optical absorbance. Measurements with grids bearing aqueous films showed that these grids experienced a temperature jump ~7% smaller than dry grids (possibly due to the greater mass and enhanced reflectivity of wet grids) and cooled faster than indicated in Fig. 2. For the 9.2-ms "flash-to-splash" interval used in most of this study, the effective temperature jump of wet grids at cryogen encounter was about 72% of the original jump measured right after the flash for jumps starting from room temperature (data not shown).

Cryo-TEM

Specimens were mounted in a Gatan 626 cold stage and examined at a cold stage temperature of −170°C in a Philips CM12 TEM at 100 keV, with a coefficient of spherical aberration of 2.0 mm. Images were obtained using low electron-dose procedures. Two successive images were obtained of each area, ~1 μm and 2 or 2.5 μm under focus, respectively. These underfocus settings were chosen to allow resolution of the leaflet structure of the bilayer and to increase the apparent contrast of the bilayer as a unit, respectively. The conditions were chosen based on the results of experience in previous studies (Siegel et al., 1989; Frederik et al., 1991) and on predicted behavior of the contrast transfer function under these conditions (summarized, for example, by Dubochet et al., 1988). In practice, the true underfocus settings were slightly different. This is partly due to errors in determining focus and partly due to the non-planarity of cryo-TEM specimens (Booy and Pawley, 1993), which results in small focus errors between the area of the specimen used for setting focus and the area that is actually exposed in the low-dose mode (10 μm away in the specimen plane under the conditions used). Images obtained under these conditions showed no apparent electron beam-induced damage or devitrification. In some experiments (data not shown), three successive images of each area could be obtained under these conditions without apparent damage. Images were recorded on Kodak SO-163 film (Eastman Kodak Co., Rochester, NY) and were developed for 12 min in undiluted Kodak D-19 developer for highest electron speed.

Liposomes

Phospholipids were obtained from Avanti Polar Lipids (Alabaster, AL) and were used without further purification. Chloroform suspensions of the lipids were rotary evaporated to dryness in glass flasks and evacuated for 1 h. Films of N-monomethylated dioleoylphosphatidylethanolamine (DOPE-Me) or dioleoylphosphatidylcholine (DOPC) were hydrated in buffer (150 mM NaCl, 20 mM *N*-tris(hydroxymethyl)methyl-2-aminoethanesulfonic acid (TES), pH 7.4, 0.1 mM EDTA) for 1 h at 0–4°C and then dispersed by vigorous vortex mixing. Specimens were also made using phosphatidylethanolamine made by transphosphatidylation of hen egg phosphatidylcholine (TPE). TPE films were treated in the same manner as the DOPE-Me films, except that the buffer was 100 mM NaCl, 5 mM glycine pH 9.9, 0.1 mM EDTA. The lipid dispersions were subjected to one of two treatments. Sonicated large unilamellar vesicles (son-LUVs) were produced by extrusion of the dispersion through 0.05-μm filters in a Lipex Biomembranes (Vancouver, Canada) high-pressure extruder and then sonicated on ice (model S-12 sonicator with microtip; Branson Sonic Power Co., Danbury, CT) for 8 cycles of 60 s ultrasonic irradiation and 60 s of cooling. Son-LUVs were generally produced within an hour of cryo-TEM sample preparation. LUVs were produced simply by extrusion of the lipid dispersion through 0.1-μm filters.

Phosphatidylethanolamine liposomes can only be prepared at high pH, where the H_{II} phase cannot form, and where the liposomes are stable with respect to aggregation and destabilization (Ellens et al., 1986, 1989). To prepare cryo-TEM specimens, 3 μl of TPE LUVs in pH 9.9 glycine buffer (composition given above) was mixed on the electron microscope grid with an equal volume of roughly iso-osmotic solution containing a 25 mM acetate buffer at pH 4.5. This rapidly lowered the pH so that H_{II} phase could form when the specimen is heated. Using the acetic acid permeation coefficient for membranes made of bacterial phosphatidylethanolamine (3.4×10^{-5} m/s, measured by Walter and Gutknecht, 1984), it can be shown that the pH inside the liposomes equilibrated with the exterior pH within several milliseconds, well before exposure of the specimens to the temperature jump.

Differential scanning calorimetry

The T_H of TPE was determined by differential scanning calorimetry (DSC) using a MicroCal MC2 (MicroCal Co., Amherst, MA) calorimeter. The TPE was equilibrated with pH 4.5 buffer for 1 h at 0°C, vigorously vortex-mixed, subjected to five freeze/thaw cycles (dry ice/45°C water bath) with resuspension via vortex mixing after every thaw, loaded into the calorimeter at ~0°C and a TPE concentration of 12 mg/ml, and scanned at 14 K/h.

RESULTS

Anticipated morphology

The intermediate structures discussed in the Introduction are drawn in Fig. 3 in the manner in which they are expected to appear in cryo-TEM images. In Fig. 3 *A*, an IMI is depicted as viewed from the side (*left*) and top (*right*). The same views are given of a stalk in Fig. 3 *B*. Note that the two apposed bilayer lamellae are deformed toward one another on the periphery of the stalk (*left*). An LD is shown in Fig. 3 *C*. Views from the side and top are given in the upper and lower parts of Fig. 3 *C*, respectively. In cross-section parallel to its long axis, an LD resembles the cross-section of the stalk given in the left part of Fig. 3 *B*. An LD can arise from either stalks or IMIs. If it arises from IMIs, the end of the LD will resemble an IMI (Fig. 3 *C*, left), while the end will resemble half of a stalk if it forms from a stalk (Fig. 3 *C*, *right*). The process of H_{II} phase formation from LDs is discussed by Siegel (1986a). An ILA resembles a catenoidal (spool-shaped) bilayer connection between two apposed bilayer lamellae (Fig. 3 *D*, side and top views given at *left* and *right*, respectively). Note that IMIs and ILAs are in principle difficult to distinguish by cryo-TEM. However, a combination of cryo-TEM and FFEM data can be used to distinguish between the two structures (Siegel et al., 1989).

DOPC

To determine whether irradiation by the flashtube produces any damage to the specimen, specimens of DOPC son-LUVs

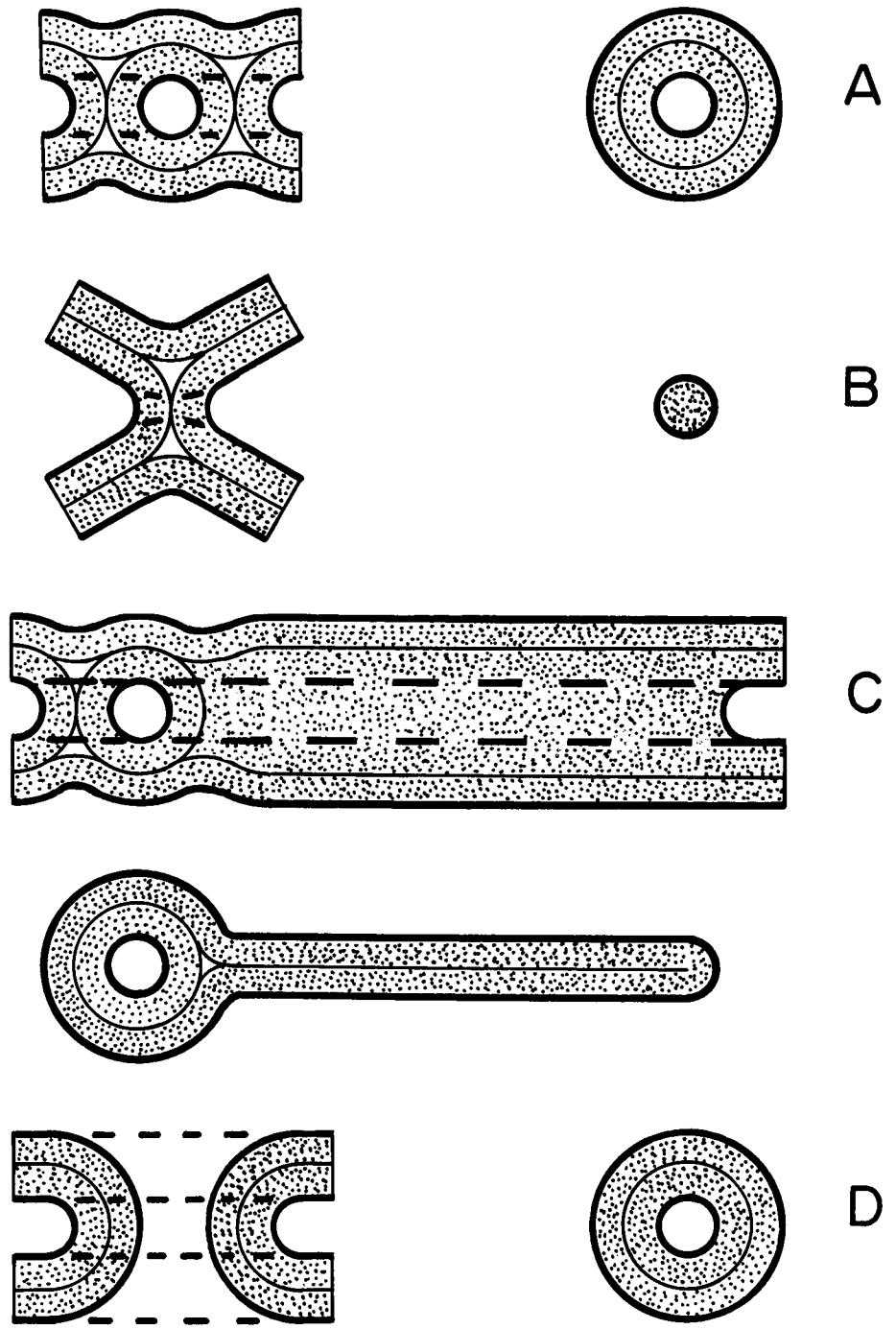

FIGURE 3 Possible intermediates in L_α/H_{II} transitions as they would appear in cryo-TEM. Lipid monolayers are drawn as slabs. The heavier lines are the lipid/water interfaces, which generate most contrast. The dashed heavy lines are the interfaces of surrounding bilayers, which are visible through the structures when viewed from the side in TEM. Generally, the parts of the structure that generate the most contrast are those in which the monolayers are parallel to the incident electron beam. (*A*) IMI, consisting of a spherical inverted micelle within a semitoroidal outer monolayer. Views are from the side (*left,* incident electrons in the plane of the L_α phase bilayers) and along the axis (*right,* observed perpendicular to the bilayers). (*B*) Stalk, a catenoidal (cusp-like) attachment between the facing monolayers of apposed bilayers. Views are from the side (*left*) and top (*right*). (*C*) LD, a type of structure common to both models of the transition process. The LD consists of a unit cell of H_{II} phase in cross-section, each end of which is terminated either by an IMI (*left*) or stalk (*right*), depending on how the LD formed. The top drawing is a view from the top (incident beam perpendicular to the L_α phase lamellae), and the bottom drawing is a view from the side. (*D*) ILA, a catenoidal bilayer attachment between apposed planar bilayers. Top and side views are given. Note that this structure may be difficult to distinguish from IMIs by cryo-TEM.

were processed in the apparatus with and without a temperature jump (Fig. 4, *A* and *B*, respectively). The initial CEVS temperature was 25°C. Based on our calibration experiments (see Materials and Methods) the estimated peak

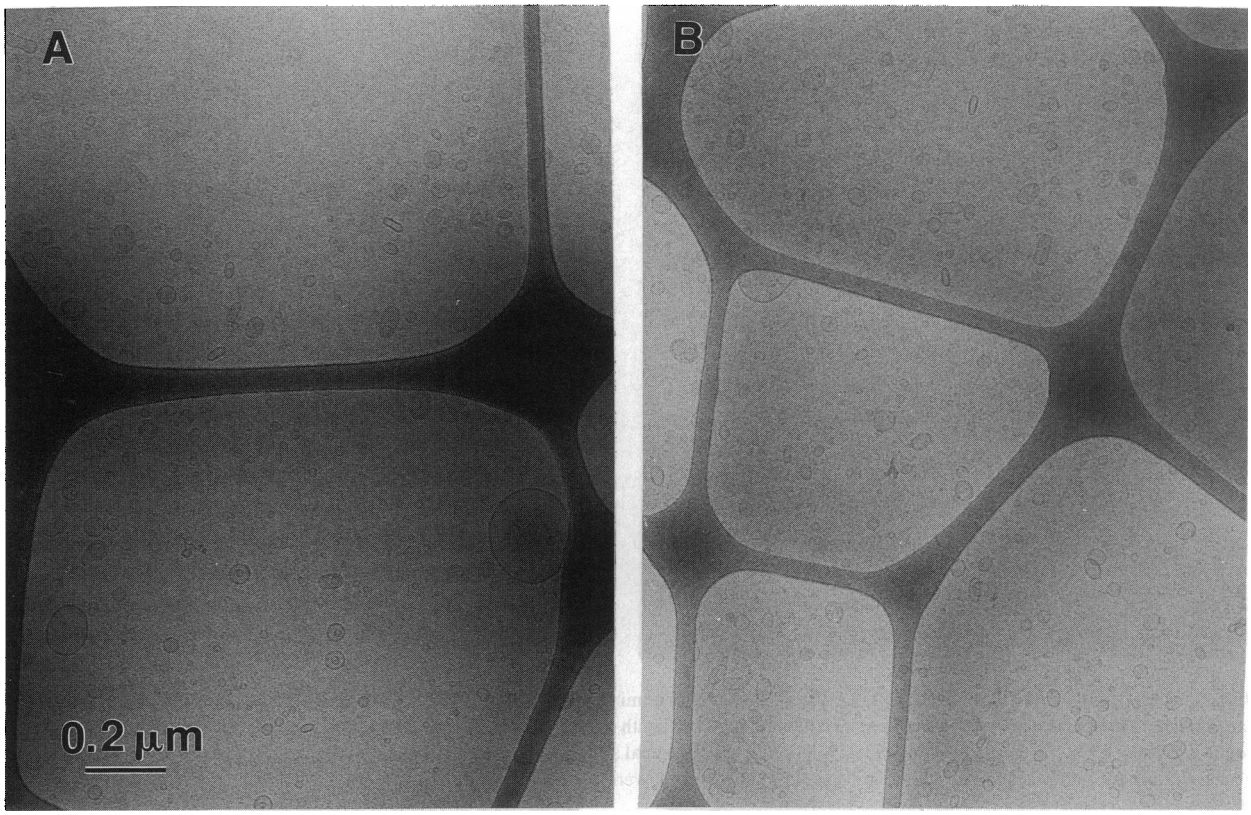

FIGURE 4 Samples of son-LUVs of DOPC without (*A*) and with (*B*) a flash-induced temperature-jump before vitrification. The initial CEVS temperature was 25°C, and the flash occurred 9.2 ms before cryogen encounter. The peak temperature and temperature at cryogen encounter were ~100°C and 76 ± 8°C, respectively. There is no obvious damage produced by exposure to the flash (*B* versus *A*). These images were obtained with the microscope set ~2 μm (*A*) and 2.5 (*B*) μm under focus.

temperature was 96–100°C, and the temperature 9 ms later, at cryogen encounter, was estimated to be 76 ± 8°C. The size distribution and general appearance of the liposomes is the same in specimens processed without (Fig. 4 *A*) and with (Fig. 4 *B*) a temperature jump. Similar results are obtained using LUVs, which are larger structures (data not shown).

TPE

TPE was chosen as an example of a lipid system that exhibits facile L_α/H_{II} phase transitions, without formation of hysteretic isotropic or inverted cubic phases. TPE samples do not exhibit isotropic ^{31}P nuclear magnetic resonance spectral components near T_H (Boggs et al., 1981; Lai et al., 1985). Such isotropic components are characteristic of systems that form significant numbers of ILAs or an inverted cubic phase (Ellens et al., 1989), as confirmed by cryo-TEM studies (Siegel et al., 1989; Frederik et al., 1991) and x-ray diffraction and DSC (Siegel and Banschbach, 1990). DSC experiments (data not shown) established the T_H of this lot of TPE as 59°C. T_H has been reported to vary by several degrees between different lots of TPE (Lai et al., 1985). The value we determined is in the center of the range determined by others (56–63°C: Boggs et al., 1981; Lai et al., 1985; Ellens et al., 1986).

The on-the-grid pH jump applied to the TPE suspension produced rapid aggregation of the TPE LUVs. Because of this, the aqueous films of the specimen were quite thick. Only a small fraction of the area of the grids was thin enough to be observed by cryo-TEM. Micrographs of these suspensions, processed at a constant temperature of 25°C (Fig. 5 *A*), show only densely packed arrays of LUVs. Specimens that were prepared identically but subjected to a temperature jump had a substantially different appearance (Fig. 5 *B*; note the change in scale with respect to Fig. 5 *A*). Areas of the grids that were thin enough to examine with cryo-TEM were nearly featureless at moderate magnification; in Fig. 5 *B*, all liposomal structures seem to have disappeared on account of the temperature jump. At higher magnification, the areas exhibited arrays of lines in swirl-like domains with spacing of 3.3–3.8 nm, roughly corresponding to the d_{11} and d_{20} spacing expected in the H_{II} phase. The specimen in Fig. 5 *B* experienced a peak temperature of ~100°C and a temperature at cryogen encounter of 82 ± 12°C, corresponding to superheating of ~41 and 23 K above T_H, respectively. Our tentative conclusion is that most of the temperature-jumped specimens had completed the L_α/H_{II} transition within the "flash-to-splash" interval of 9.2 ms. Recently, S. Gruner and co-workers (manuscript in preparation) have also observed L_α/H_{II} transitions occurring within <9 ms in DOPE speci-

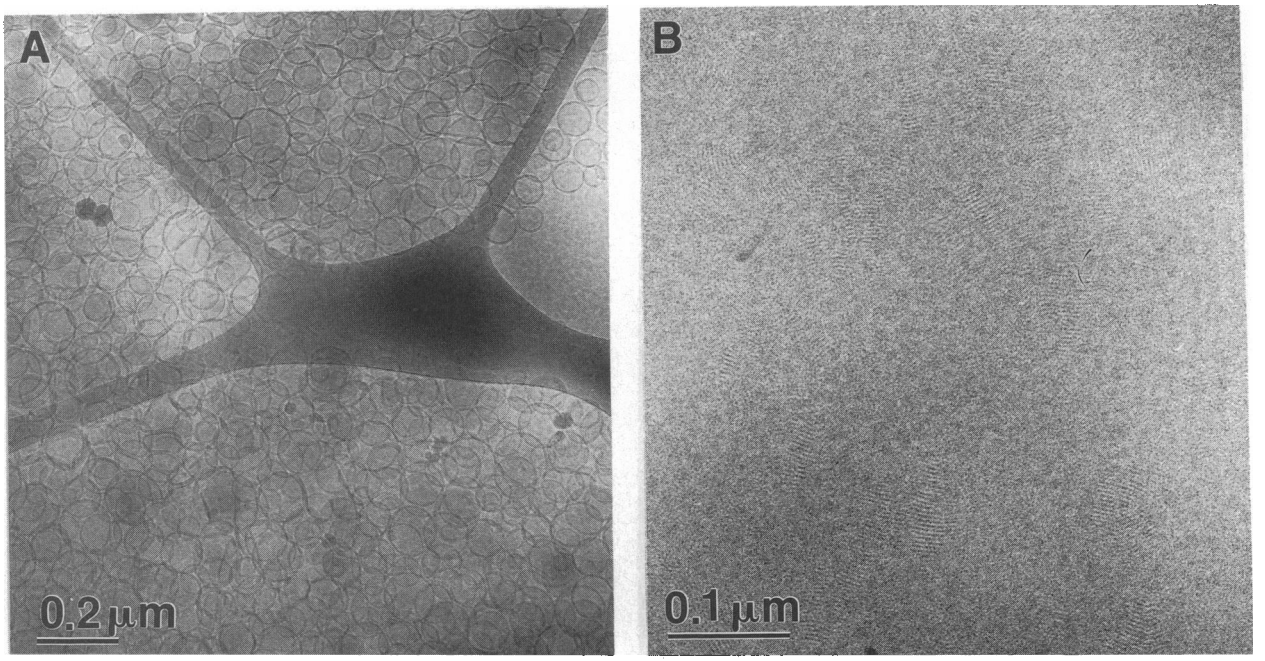

FIGURE 5 The L_α/H_{II} phase transition in TPE LUVs. TPE LUVs were mixed with pH 4.5 buffer on the grid at 23°C to enable the transition to occur upon an increase in temperature. Samples were processed without (*A*) and with (*B*) a temperature jump (estimated peak temperature of ~100°C, temperature at cryogen encounter 82 ± 12°C). T_H for this lipid is 59°C. In *B*, the liposomal structures are gone. The swirl-like arrays of lines appear to represent domains of H_{II} phase. Note the increase in scale in *B* relative to *A*. These images were obtained with the microscope set ~1 μm under focus.

mens that experience rapid reductions in pressure from several kilobars to one bar.

DOPE-Me

The extensive liposome aggregation that occurred during the pH jump made TPE LUVs difficult to work with. Moreover, the transition in TPE appeared to be too fast to study with this apparatus, at least with extensive superheating. Therefore, further studies were made using DOPE-Me. DOPE-Me forms isotropic and inverted cubic phases around T_H (Gagné et al., 1985; Gruner et al., 1988; Siegel and Banschbach, 1990). This is expected to slow the L_α/H_{II} phase transition due to interference of ILAs in close apposition of large amounts of L_α phase membranes (Siegel, 1986a-c) and, presumably, diversion of some of the initial intermediates into ILA formation (as opposed to H_{II} precursor formation). DOPE-Me is also a more tractable system for TRC-TEM, because liposomes of DOPE-Me aggregate much less rapidly than TPE liposomes at neutral pH and room temperature (Ellens et al., 1986, 1989). LUVs and son-LUVs made in pH 7.4 buffer immediately before the TRC-TEM experiment and stored on ice did not aggregate very extensively, so that cryo-TEM specimens with usable film thickness could be made at room temperature without the pH jump procedure used for TPE LUVs.

DOPE-Me LUVs and son-LUVs were consistently larger and contained a larger number of oligomeric structures than preparations of DOPC made in the same way. Fig. 6 *A* is a micrograph of DOPE-Me son-LUVs made by the same protocol as the DOPC son-LUVs in Fig. 4 *A*. The DOPE-Me structures are 0.05–0.2 μm or more in diameter, and many are oligolamellar, while most of the DOPC son-LUVs are unilamellar and only 0.02 to 0.06 μm in diameter.

Fig. 6 *B* is a micrograph of a DOPE-Me son-LUV dispersion identical to the one in Fig. 6 *A* that was subjected to a temperature jump, producing a peak temperature of 90 ± 10°C and a temperature at cryogen encounter of 71 ± 7°C. The T_H of DOPE-Me is 66°C (Siegel and Banschbach, 1990), so these temperatures correspond to superheating by 24 ± 10 and 5 ± 7 K, respectively. The smaller degree of superheating was chosen to slow the transition further relative to the rapid transition in TPE. The most striking features of Fig. 6 *B* relative to Fig. 6 *A* are that the liposomal structures are much larger and that there is a large number of structures previously identified as ILAs (Siegel et al., 1989; Frederik et al., 1991), viewed either from the side (*arrow*) or down the pore axis (*arrowhead*). Fig. 7 presents two views of ILA arrays in specimens of DOPE-Me LUVs treated in the same way as Fig. 6 *B*. The initial liposomes were larger and more oligolamellar than in the son-LUVs of Fig. 6 *A* (data not shown). In both Figs. 6 *B* and 7, the original liposomes fused into larger structures and formed numerous ILAs within the 9.2-ms "flash-to-splash" interval. ILA formation between liposomes corresponds to membrane fusion (Ellens et al., 1989; Siegel et al., 1989), so the growth in liposome size is due to ILA production.

As discussed above, a rigorous distinction between ILAs and IMIs may not be possible using only cryo-TEM data, since these structures would look almost alike in all orientations (Fig. 3, *A* and *D*). Two observations suggest that the catenoidal structures in Figs. 6 *B* and Fig. 7 are ILAs. First,

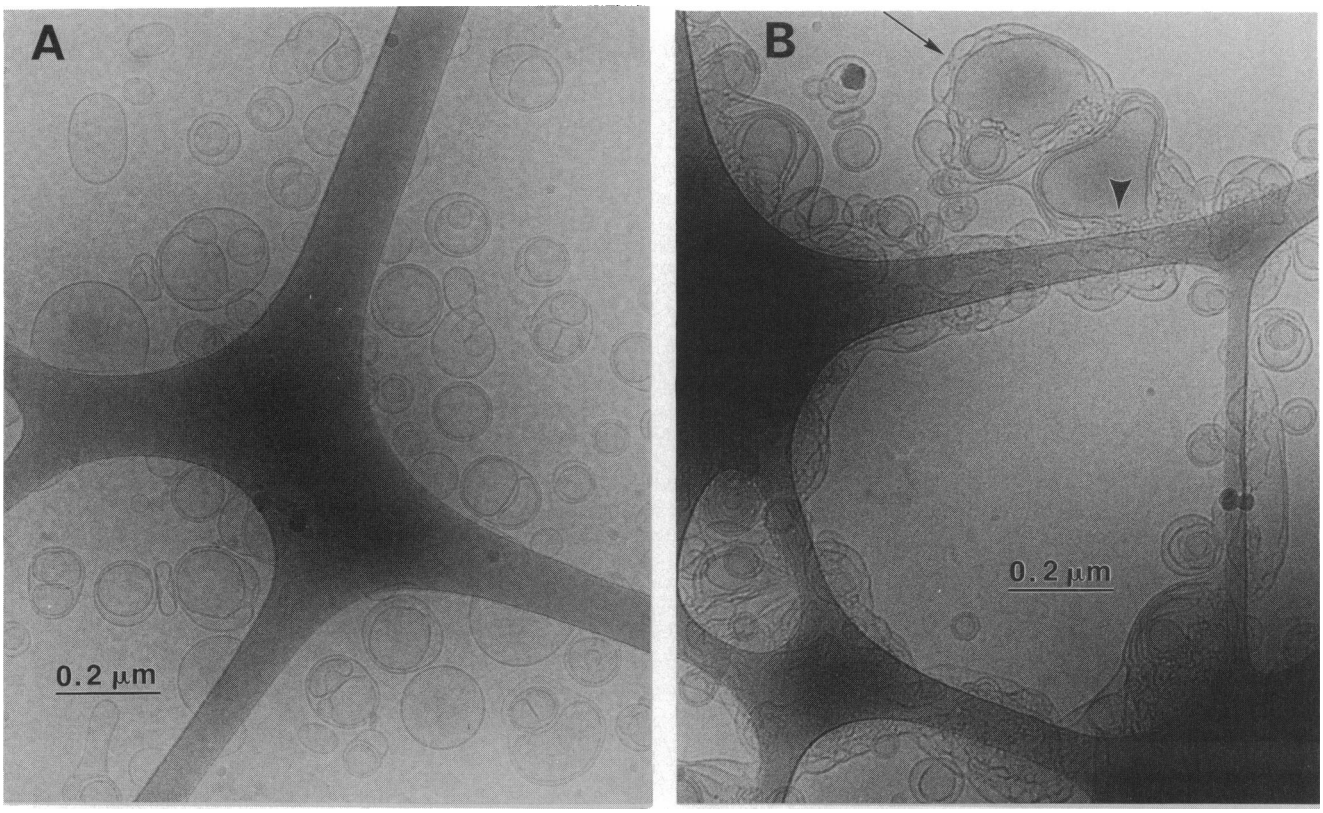

FIGURE 6 Rapid ILA formation in DOPE-Me. Son-LUVs of DOPE-Me at 23°C without (*A*) and with (*B*) a temperature jump (estimated peak temperature and temperature at cryogen encounter of 90 ± 10°C and 71 ± 7°C, respectively). T_H for this lipid is 66°C (Siegel and Banschbach, 1990). In *A*, note that although these son-LUVs were made with the same protocol as the DOPC son-LUVs in Fig. 5, the average size and proportion of oligolamellar liposomes is much larger in the DOPE-Me suspension. In *B*, note that the average size of the liposomes has increased and that many ILAs have appeared within the 9.2-ms post-flash interval. ILAs are visible in side views (*arrow*) and views down the pore axis (*arrowhead*). These images were obtained with the microscope set ~1.5 μm (*A*) and 2 μm (*B*) under focus.

parallel TRC-TEM and FFEM experiments on a very similar system by Siegel et al. (1989) indicated that this morphology arises from ILAs, because the fracture faces showed evidence of water channels on the axis of the catenoids, whereas an IMI structure would have yielded hemispherical depressions and protuberances. Second, the dimensions of the catenoidal structures we observed in these specimens were large and variable. The separation of the lipid/water interfaces of the bilayers at the periphery of the catenoids is ~13 nm and occasionally more. The pore cross-section is 7–13 nm or more. Theoretical work (Siegel, 1993) shows that IMIs should have a substantially smaller apparent pore diameter (corresponding to the diameter of the water core of the inverted micelle) of about 4 nm. Moreover, the inter-bilayer spacing at the periphery of the IMIs should also be only about 4 nm. Finally, the energy of IMIs is sensitive to their dimensions. Thus, IMIs would be expected to have a narrow range of dimensions, unlike the broad distribution of sizes observed for the catenoidal structures. In contrast, the same theoretical work shows that ILAs would be quite stable at the observed dimensions of the catenoidal structures. Moreover, the energy of ILAs is expected to be much less sensitive to ILA dimensions.

Fig. 8 is a micrograph of another DOPE-Me son-LUV specimen exposed to the same temperature jump as the specimen in Fig. 6 *B*. In this case, small domains of H_{II} phase are visible, either with the tubes in cross-section (*arrow*) or with layers of tubes viewed side-on (*arrowhead*). Presumably, this sample was heated somewhat higher relative to T_H than the one in Fig. 6 *B*, due to variations in grid weight and grid-serrefine contact area. This result shows that even with comparatively little superheating the L_α/H_{II} phase transition can proceed to an appreciable extent in only 9.2 ms in these DOPE-Me specimens.

Difficulties in imaging stalk intermediates

About 1% of the exposures taken of temperature-jumped DOPE-Me dispersions contained instances that might be interpreted as consistent with stalk morphology. However, in each case, the morphology could be explained in terms of a fortuitous juxtaposition of normal membranous structures. An example is given in Fig. 9 *A*. The arrowhead indicates what could be an intermembranous cusp with a diameter of about one bilayer width at the most narrow point, consistent with a stalk viewed side-on (Fig. 3 *B, left*). However, as illustrated in Fig. 9 *B*, the same morphology would be expected if the two liposomes in the figure were invaginated, as a substantial fraction of liposomes are in such specimens. In this case, the "stalk" would actually be an edge of the lip

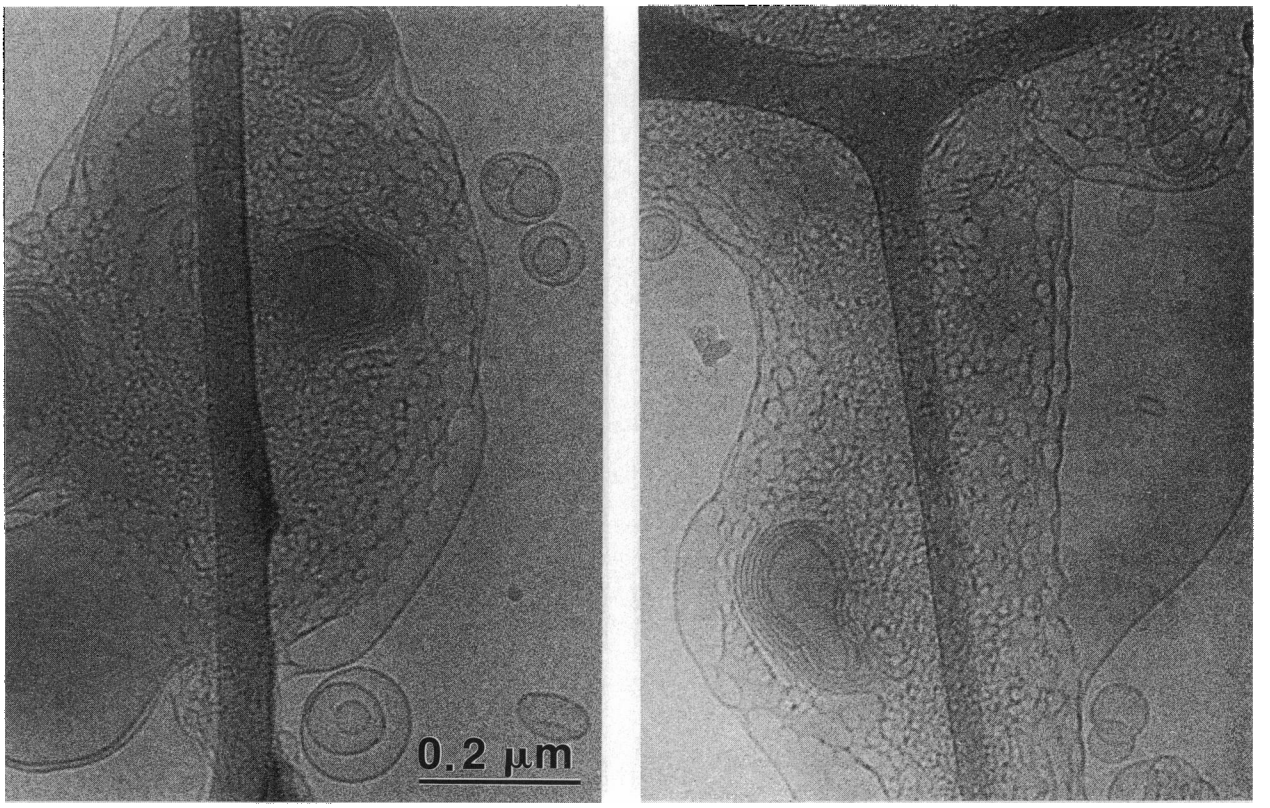

FIGURE 7 Two temperature-jump exposures similar to Fig. 6 *B* but obtained using DOPE-Me LUVs. Note the higher density of ILAs forming in these LUV as compared with son-LUV samples. These images were obtained with the microscope set ~2 μm under focus.

of the invaginated membrane of the larger liposome. We conclude that this feature is unlikely to arise from a stalk. We observed only a handful of other instances, each similarly ambiguous.

Fig. 9 *A* indicates that the limiting factor in detecting stalks, if they are present, is the poor contrast generated by the narrow "waist" of the stalk at the small degree of underfocus needed to adequately resolve the elements of the structure. The resolution of the present method is sufficient to verify the dimension of the inter-bilayer connection. A stalk should have a waist diameter equal to a bilayer thickness (Fig. 3 *B*), and the two leaflets of the bilayer membranes are well-resolved in Fig. 9 *A*. The contrast limitation is made more obvious in Fig. 9, *C* and *D*. These are two prints of regions from the same negative, both printed under exactly the same conditions, that represent areas about 1 μm apart in the specimen. The pair of arrowheads in Fig. 9 *C* indicate liposomes with sharply defined membrane edges. The pairs of small arrows each indicate nearby liposomes with the same projected diameter but much less distinct membrane edges. Presumably, these latter liposomes are lenticular in shape and have a smaller radius of curvature at the rims. In Fig. 9 *D*, the large arrowhead indicates a pair of invaginated (bowl-shaped) liposomes facing each other along the axis of the invaginations, seen edge-on. The cross-section of the rims of the invaginations show that one radius of curvature of the membranes at the rims is quite small (~6 nm). The membrane edges in this case (*small arrow*) are nearly invisible. Therefore, it appears that the contrast generated by a membrane seen edge-on is a function of the local radii of curvature of the membrane. This would make stalks, which have very small radii of curvature, very difficult to detect via cryo-TEM (see Discussion).

LDs in a kinetically trapped configuration

No structure that unambiguously resembled LDs in the plane of the specimen films (lower part of Fig. 3 *C*) was observed. However, structures that had the same cross-section as LDs were observed in a few exposures. These structures usually occurred around the periphery of liposome-liposome contacts. An example is shown in Fig. 10. The cross-sections of the LD (seen edge-on at the periphery of the liposome-liposome contact) are indicated by arrowheads. The symmetry of the liposome-liposome contacts implies that these LDs are circular; no LD ends were evident in these side-on views. If this is the case, then these LDs are closed-ring structures in which the two ends (derived from stalks, IMIs, or some other structure) have fused together. Both stalk or IMI-like ends are very unstable (Siegel, 1993). Thus there is a driving force for fusion of the ends of the LD. In a closed-ring configuration, the LD would not be free to revert to bilayer structure, since it must have free ends in order to contract as lipid diffuses out of the LD into the contiguous bilayers (Siegel, 1986a). This might explain why these putative closed-ring LDs are visible and the inferred LDs with

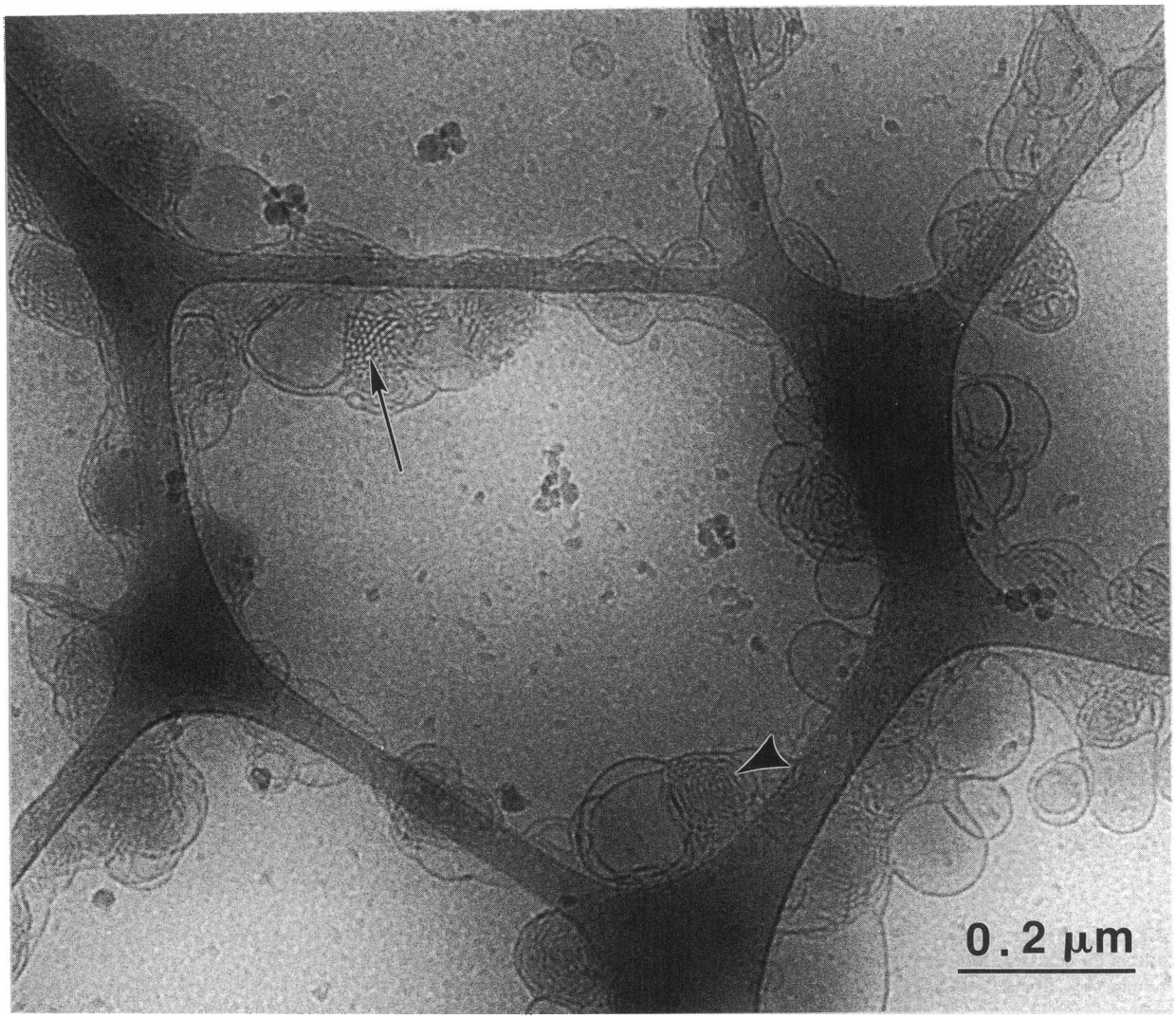

FIGURE 8 H_{II} phase domain formation in temperature-jumped DOPE-Me son-LUVs. The samples were treated as in Fig. 6. This specimen may have reached a higher temperature than the specimen in Fig. 6 due to the cited range of variability in magnitude of the temperature jump relative to T_H. Note that small domains of H_{II} tubes are visible either in cross-section (*arrow*) or from the side (*arrowhead*). The background mottling is due to contamination of the surface of the vitrified film. This image was obtained with the microscope set ~1 μm below focus.

free ends are not: LDs with unfused ends could rapidly shorten and convert back into the L_α phase during the initial cooling upon contact with cryogen.

DISCUSSION

The structure of the first intermediates in the L_α/H_{II} transition would determine which (or if either) of the two previously proposed transition mechanisms was more likely. Unfortunately, in this study the first intermediate structures could not be imaged: unambiguous examples of IMIs or stalks, or of stalk- or IMI-like ends of LDs, were not detected. However, we were able to collect data indicating the transition is more likely to proceed via a stalk-mediated than an IMI-mediated mechanism.

Two factors limit our ability to detect stalks and IMIs. First, in the case of stalks, structures of the expected size and shape of stalks could be very difficult to detect due to low image contrast, as illustrated in Fig. 9 *C*. This is a micrograph of a temperature-jumped DOPE-Me son-LUV dispersion, printed in continuous tone. Note that the membrane edges of the two liposomes indicated by pairs of small arrows generate very little contrast compared to the membrane edges of a nearby liposome of roughly the same diameter (*large arrow*). Additionally, note the two bowl-shaped, invaginated liposomes oriented with the invaginations facing each other (*arrowhead*); the edges of the membranes at the high-curvature lips of the invagination in each liposome are just barely discernible around the rim of the contact. These variations in contrast are presumably due to the different radii of curvature of the membranes in each structure. The smaller the radius of curvature in the plane perpendicular to the specimen plane, the shorter the distance the electrons travel through the membrane, and the smaller is the projected mean inner potential difference along this ray and a ray of the same length through water. This results in a smaller contribution

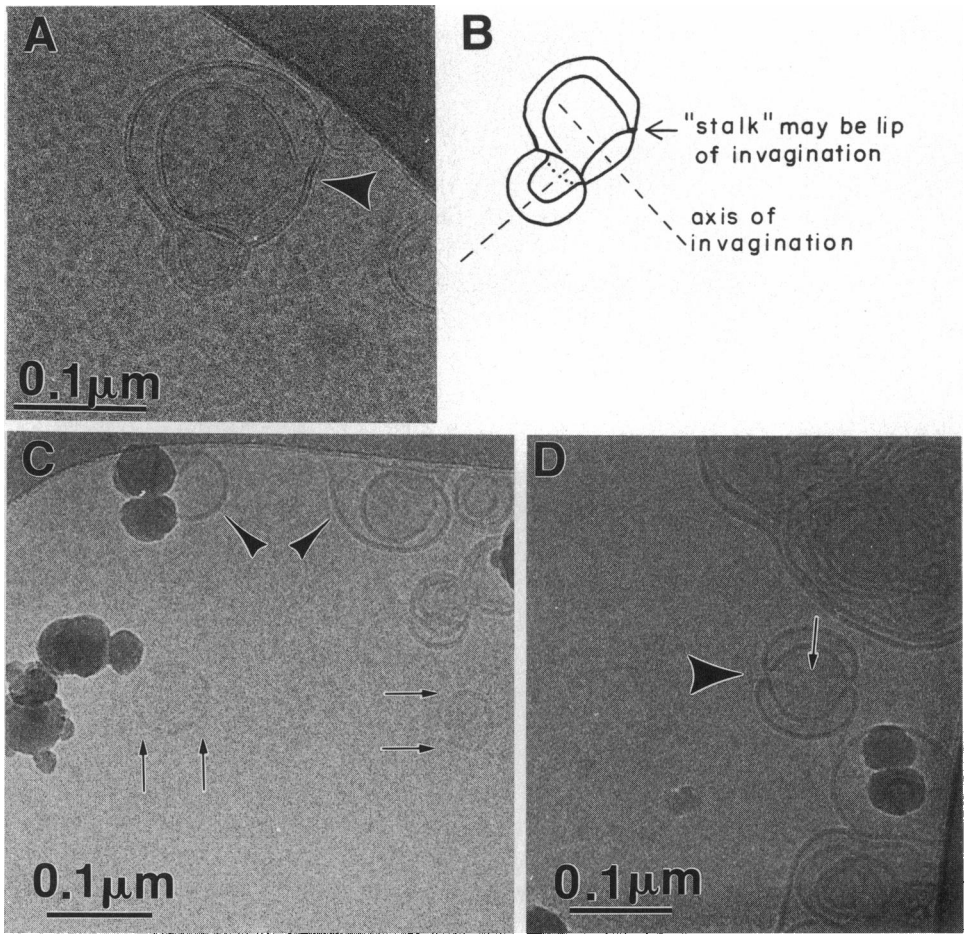

FIGURE 9 Limitations on stalk detectability imposed by superposition effects and contrast. (*A*) Morphology that is superficially consistent with a stalk viewed from the side (Fig. 3 *B, left*). (*B*) Alternative (and more likely) interpretation of the morphology in *A* as the lip of an invagination in a liposome, seen from the side. The set underfocus is 0.6 μm. (*C* and *D*) Examples of how the contrast developed by the edges of bilayer membranes decreases with decreasing radii of curvature. The sample is a dispersion of son-LUVs of DOPE-Me treated as in Fig. 5 *B*. These two micrographs are of regions that are about 1 μm apart on the same negative and were printed using exactly the same conditions at uniform tone. These images indicate that the contrast generated by membranes seen edge-on decreases rapidly as the radii of curvature of the membranes decrease (see text). The underfocus for *C* and *D* is ~1 μm.

of electrons on this path to phase contrast in the image. The liposomes indicated by small double arrows are probably lenticular structures with high-curvature edges at the periphery of the structure, whereas the liposome indicated by the large arrow is probably almost spherical. The minor radius of curvature of the bilayer membranes at the lips of the invaginations in the pair of aggregated liposome is only ~6 nm, and these folds of membrane are barely discernible edge-on. By comparison, stalks are much narrower structures (diameter of ~4 nm), and would generate even less contrast at this low degree of underfocus, which is necessary to achieve the required resolution. If they exist, stalks would be very difficult to detect via this method. The most visible feature of stalks would be the deformation of the bilayers at the periphery of the stalk.

Second, both IMIs and stalks may be able to revert to bilayer structure on sub-microsecond time scales (Siegel, 1986a, 1993), especially when subjected to large degrees of supercooling immediately after specimen contact with the cryogen. As noted in Materials and Methods, it may take

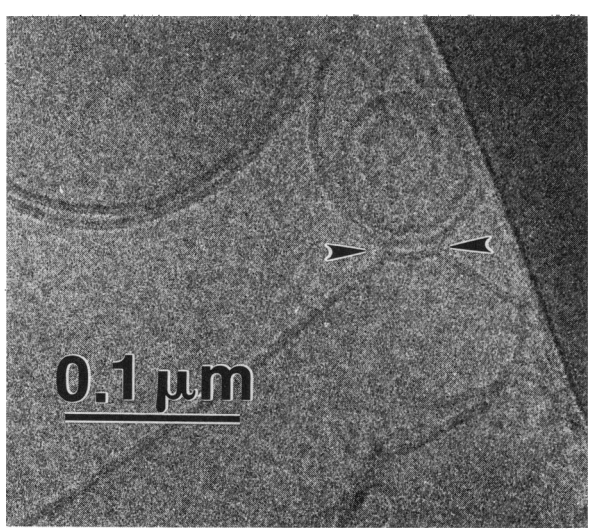

FIGURE 10 Ring-shaped LD formed between apposed DOPE-Me liposomes in temperature-jumped DOPE-Me son-LUVs (treated as in Fig. 5 *B*). The arrowheads indicate the locations where the LD is seen in cross-section. See text. The underfocus is ~1 μm.

as much as 1 ms for the specimen to cool to the point at which vitrification occurs. LDs are also expected to shorten rapidly to their original (IMI or stalk-like) dimensions on that time scale (Siegel, 1986a). This may be the reason that the only LD-like structures that we observed appear to be closed-ring LDs that are inhibited from shortening in that manner (Fig. 10).

Two of our findings suggest that lamellar/inverted phase transitions are more likely to proceed via stalks than via IMIs. First, the L_α/H_{II} transition in systems like TPE (which does not form isotropic or inverted cubic phases) can be very fast. In our experiments, superheating to 23–41 K above T_H produced transitions that were complete within the "flash-to-splash" interval of 9.2 ms (Fig. 5 *B*). L_α/H_{II} transitions in less than 9 ms have also been observed via time-resolved x-ray diffraction in DOPE (S. Gruner et al., manuscript in preparation). The IMI-mediated transition mechanism (Siegel, 1986a) proceeds in three stages: IMI production, IMI aggregation and LD formation, and LD elongation. The first and last stages could be fast (millisecond time scales for substantial degrees of superheating; Siegel, 1986a). The last stage, LD elongation, is the most rapid phase of the transition process. However, the middle stage is a two-dimensional aggregation process, and such processes tend to be slow (Torney and McConnell, 1983). The IMI mechanism suggested by Siegel (1986a) is barely capable of generating transitions at the observed rates, but the parameters have to have optimal values in order for it to do so. Moreover, some of the assumptions used in deriving the kinetic analysis in Siegel (1986a) have to be questioned in the light of more recent results (Siegel, 1993). In contrast, in a stalk-mediated mechanism, the stalks themselves are capable of immediately forming LDs, without a slow aggregation step. The transition time in a stalk mechanism is limited by the stalk production and LD elongation rates, both of which should occur on millisecond time scales or faster (Siegel, 1986a; 1993). Hence a stalk-mediated transition like the mechanisms proposed by Hui et al. (1983) and Caffrey (1985) is more compatible with the fast transition times that are observed. The second factor that favors a stalk-mediated mechanism is the appearance of large numbers of ILAs in DOPE-Me son-LUVs or LUVs within the same 9.2-ms interval (Figs. 6 *B* and 7). The number of ILAs produced appears to be limited mainly by the proportion of membrane area that is closely apposed, since the ILAs are more numerous in the LUV samples, which had a larger fraction of oligolamellar liposomes (Fig. 7). An earlier kinetic analysis (Siegel, 1986a-c) indicated that ILAs should form slowly from individual IMIs with characteristic times of ~1 s for lipids like DOPE-Me, although these calculations are sensitive to the values of input parameters. In contrast, for systems like DOPE-Me, stalks should form ILAs rapidly since no significant lipid concentration fluctuation in the stalk is required and ILAs have substantially lower energies than stalks (Siegel, 1993). The relative rates of ILA and LD formation in a stalk-mediated transition cannot be predicted but are probably controlled by the details of the stalk rearrangement process and small differences in stalk and ILA curvature energy between systems like TPE and DOPE-Me.

The contrast in our images is low, and the signal-to-noise ratio is rather poor. In future work, it may be useful to use image analysis techniques to enhance contrast. In addition, some transmission electron microscopes are now equipped with energy filters. These filters increase the signal-to-noise ratio by eliminating inelastically scattered electrons.

The present study shows that TRC-TEM experiments can be performed on a millisecond time scale. Experiments on this time scale should be very useful in the study of dynamic phenomena in membranes, large protein complexes, and other colloidal dispersions. TRC-TEM is most effective when applied to systems in which the dynamic morphology of interest forms images with significant contrast (i.e., in lipid/water systems, dimensions $\geq$ bilayer thickness) and which is stable on the time scale of sample precooling and vitrification (<1 ms). Both of these criteria are met, for example, by the complexes of membrane fusion-catalyzing proteins involved in viral infection and exocytosis (Bentz, 1993; White, 1992): patch-clamp experiments indicate that the pore formation times and lifetimes are on the order of milliseconds, and the pore structures have dimensions of 10 nm or more. Fast TRC-TEM should yield insight into the fusion mechanisms in such systems through information concerning the time-dependent structure of the protein complex and fusion pores. Hand-mixing TRC-TEM studies of such systems are already bearing fruit (Booy, 1993).

REFERENCES

Bayly, J. G., V. B. Kartha, and W. H. Stevens. 1963. The absorption spectra of liquid phase H_2O, HDO and D_2O from 0:7 microns to 10 microns. *Infrared Physics.* 3:211–223.

Bellare, J. R., H. T. Davis, L. E. Scriven, and Y. Talmon. 1988. Controlled environment vitrification system: an improved sample preparation technique. *J. Electron Microsc. Tech.* 10:87–111.

Bentz, J, editor. 1993. Viral Fusion Mechanisms. CRC Press, Boca Raton, FL.

Bird, R. B., W. E. Stewart, and E. N. Lightfoot. 1960. Transport Phenomena. John Wiley & Sons, New York. 356–357.

Boggs, J. M., D. Stamp, D. W. Hughes, and C. M. Deber. 1981. Influence of ether linkage on the lamellar to hexagonal phase transition of ethanolamine phospholipids. *Biochemistry.* 20:5728–5735.

Booy, F. 1993. Cryoelectron microscopy. *In* Viral Fusion Mechanisms. J. Bentz, editor. CRC Press, Boca Raton, FL. 21–54.

Booy, F. P., and J. B. Pawley. 1993. Cryo-crinkling: what happens to carbon films on copper grids at low temperature. *Ultramicroscopy.* 48:273–280.

Caffrey, M. 1985. Kinetics and mechanism of the lamellar gel/lamellar liquid crystal and lamellar/inverted hexagonal phase transition in phosphatidylethanolamine: a real-time x-ray diffraction study using synchrotron radiation. *Biochemistry.* 24:4826–4844.

Chestnut, M. H., D. P. Siegel, J. L. Burns, and Y. Talmon. 1992. A temperature-jump device for time-resolved cryo-transmission electron microscopy. *Microsc. Res. Tech.* 20:95–101.

Clark, J., P. Echlin, R. Moreton, A. Saubermann, and P. Taylor. 1976. Thin film thermocouples for use in scanning electron microscopy. *In* Scanning Electron Microscopy/1976, Proceedings of the Ninth Annual Scanning Electron Microscope Symposium. Vol. 1. O. Johari, editor. IIT Research Institute, Chicago. 83–90.

Dubochet, J., M. Adrian, J.-J. Chang, J.-C. Homo, J. Lepault, A. McDowall, and P. Schultz. 1988. Cryo-electron microscopy of vitrified specimens. *Q. Rev. Biophys.* 21:129–228.

Ellens, H., J. Bentz, and F. C. Szoka. 1986. Destabilization of phosphatidylethanolamine liposomes at the hexagonal phase transition temperature. *Biochemistry*. 25:285–294.

Ellens, H., D. P. Siegel, D. Alford, P. L. Yeagle, L. Boni, L. J. Lis, P. J. Quinn, and J. Bentz. 1989. Membrane fusion and inverted phases. *Biochemistry*. 28:3692–3703.

Frederik, P. M., M. C. A. Stuart, and A. J. Verkleij. 1989. Intermediary structures during membrane fusion as observed by cryo-electron microscopy. *Biochim. Biophys. Acta*. 979:275–278.

Frederik, P. M., K. N. J. Burger, M. C. A. Stuart, and A. J. Verkleij. 1991. Lipid polymorphism as observed by cryo-electron microscopy. *Biochim. Biophys. Acta*. 1062:133–141.

Gagné, J., L. Stamatatos, T. Diacovo, S. W. Hui, P. L. Yeagle, and J. R. Silvius. 1985. Physical properties and surface interactions of bilayer membranes containing N-methylated phosphatidylethanolamines. *Biochemistry*. 24:4400–4408.

Gruner, S. M., M. W. Tate, G. L. Kirk, P. T. C. So, D. C. Turner, D. T. Keane, C. P. S. Tilcock, and P. R. Cullis. 1988. X-ray diffraction study of the polymorphic phase behavior of N-mono-methylated dioleoylphosphatidylethanolamine. *Biochemistry*. 2&:2853–2866.

Hui, S. W., T. P. Stewart, and L. T. Boni. 1983. The nature of lipidic particles and their roles in polymorphic transitions. *Chem. Phys. Lipids*. 33:113–126.

Laggner, P., M. Kriechbaum, and G. Rapp. 1991. Structural intermediates in phospholipid phase transitions. *J. Appl. Cryst.* 24:836–842.

Lai, M.-Z., W. J. Vail, and F. C. Szoka. 1985. Acid- and calcium-induced structural changes in phosphatidylethanolamine membranes stabilized by cholesteryl hemisuccinate. *Biochemistry*. 24:1654–1661.

Lindblom, G., and L. Rilfors. 1989. Cubic phases and isotropic structures formed by membrane lipids—possible biological relevance. *Biochim. Biophys. Acta*. 988:221–256.

Markin, V. S., M. M. Kozlov, and V. L. Borovjagin. 1984. On the theory of membrane fusion. The stalk mechanism. *Gen. Physiol. Biophys.* 5:361–377.

Siegel, D. P. 1984. Inverted micellar structures in bilayer membranes: formation rates and half-lives. *Biophys. J.* 45:399–420.

Siegel, D. P. 1986a. Inverted micellar intermediates and the transitions between lamellar, cubic, and inverted hexagonal lipid phases. I. Mechanism of the $L_\alpha \leftrightarrow H_{II}$ phase transitions. *Biophys. J.* 49:1155–1170.

Siegel, D. P. 1986b. Inverted micellar intermediates and the transitions between lamellar, cubic, and inverted hexagonal lipid phases. II. Implications for membrane-membrane interactions and membrane fusion. *Biophys. J.* 49:1171–1183.

Siegel, D. P. 1986c. Inverted micellar intermediates and the transitions between lamellar, cubic, and inverted hexagonal amphophile phases. III. Isotropic and inverted cubic state formation via intermediates in transitions between L_α and H_{II} phases. *Chem. Phys. Lipids*. 42:279–301.

Siegel, D. P. 1993. The energetics of intermediates in membrane fusion: comparison of stalk and inverted micellar intermediate mechanisms. *Biophys. J.* 65:2124–2140.

Siegel, D. P., and J. L. Banschbach. 1990. Lamellar/inverted cubic (L_α/Q_{II}) phase transition in N-methylated dioleoylphosphatidyl- ethanolamine. *Biochemistry*. 29:5975–5981.

Siegel, D. P., J. L. Burns, M. H. Chestnut, and Y. Talmon. 1989. Intermediates in membrane fusion and bilayer/non-bilayer phase transitions imaged by time-resolved cryo-transmission electron microscopy. *Biophys. J.* 56:161–169.

Talmon, Y., J. L. Burns, M. H. Chestnut, and D. P. Siegel. 1990. Time-resolved cryo-transmission electron microscopy. *J. Electron Microsc. Tech.* 14:6–12.

Tate, M. W., E. Shyamsunder, S. M. Gruner, and K. L. D'Amico. 1992. Kinetics of the lamellar-inverse hexagonal phase transition determined by time-resolved x-ray diffraction. *Biochemistry*. 31:1081–1092.

Torney, D. C., and H. M. McConnell. 1983. Diffusion-limited reaction rate theory for two-dimensional systems. *Proc. R. Soc. Lond. (Biol)* A387: 147–170.

Van Venetië, R., and A. J. Verkleij. 1981. Analysis of the hexagonal II phase and its relations to lipidic particles and the lamellar phase. A freeze-fracture study. *Biochim. Biophys. Acta*. 645:262–269.

Verkleij, A. J. 1984. Lipidic intramembranous particles. *Biochim. Biophys. Acta*. 779:43–63.

Verkleij, A. J., C. J. A. Van Echteld, W. J. Gerritsen, P. R. Cullis, and B. De Kruijff. 1980. The lipidic particle as an intermediate structure in membrane fusion processes and bilayer to hexagonal H_{II} phase transitions. *Biochim. Biophys. Acta*. 600:620–624.

Walter, A., and J. Gutknecht. 1984. Monocarboxylic acid permeation through lipid bilayer membranes. *J. Membrane Biol.* 77:255–264.

White, J. M. 1992. Membrane fusion. *Science (Washington DC)* 258:917–924.